Spatiotemporal gradients of intra-axonal [Na^+] after transection and resealing in lizard peripheral myelinated axons

Gavriel David, John N. Barrett and Ellen F. Barrett

Department of Physiology and Biophysics R-430, University of Miami School of Medicine, PO Box 016430, Miami, FL 33101, USA

1. Post-transection changes in intracellular Na^+ ($[Na^+]_i$) were measured in lizard peripheral axons ionophoretically injected with the Na^+-sensitive ratiometric dye, sodium-binding benzofuran isophthalate (SBFI).

2. Following axonal transection in physiological saline $[Na^+]_i$ increased to more than 100 mM in a region that quickly extended hundreds of micrometres from the transection site. This post-transection increase in $[Na^+]_i$ was similar when the bath contained 5 μM tetrodotoxin, but was absent in Na^+-free solution. Depolarization of uncut axons in 50 mM K^+ produced little or no elevation of $[Na^+]_i$ until veratridine was added. These results suggest that the post-transection increase in $[Na^+]_i$ was due mainly to Na^+ entry via the cut end, rather than via depolarization-activated Na^+ channels.

3. The spatiotemporal profile of the post-transection increase in $[Na^+]_i$ could be accounted for by movement of Na^+ from the cut end with an apparent diffusion coefficient of $1{\cdot}3 \times 10^{-5}$ cm^2 s^{-1}.

4. $[Na^+]_i$ began to decline toward resting levels by 20 ± 15 min (mean $\pm$ S.D.) post-transection, except in regions of the axon within 160 ± 85 μm of the transection site, where $[Na^+]_i$ remained high. The boundary between axonal regions in which $[Na^+]_i$ did or did not recover probably defines a locus of resealing of the axonal membrane.

5. $[Na^+]_i$ returned to resting values within about 1 h after resealing, even in axonal regions where the normal transmembrane $[Na^+]$ gradient had completely dissipated. The recovery of $[Na^+]_i$ was faster and reached lower levels than expected by diffusional redistribution of Na^+ along the axon. Partial recovery occurred even in an isolated internode, indicating that the internodal axolemma can actively extrude Na^+.

Peripheral axons usually regenerate after transection, but relatively little is known about the initial stages of their recovery. Transection allows normally membrane-impermeant dyes to enter the axon (Xie & Barrett, 1991), and disrupts transmembrane ionic gradients, causing axonal depolarization and increases in intra-axonal [Ca^{2+}] (Meiri, Spira & Parnas, 1981; Yawo & Kuno, 1985; Lucas, Gross, Emery & Gardner, 1985; Strautman, Cork & Robinson, 1990; Berdan, Easaw & Wang, 1993; Spira, Benbassat & Dormann, 1993; Zev & Spira, 1993; Krause, Fishman, Ballinger & Bittner, 1994). At some point in the recovery process the axonal membrane must reseal, permitting restoration of normal transmembrane ionic gradients. The time course of membrane resealing has been estimated by electrophysiological criteria, such as the time required to restore the axonal resting potential and input resistance (Yawo & Kuno, 1985) or the time required for injury currents to subside (Borgens, Jaffe & Cohen, 1980; Krause *et al.* 1994). Other studies have measured the time required to regain the ability to exclude or retain membrane-impermeant dyes (Xie & Barrett, 1991; Steinhardt, Bi & Alderton, 1994), or to form a tightly packed vesicular plug at the cut end (Krause *et al.* 1994).

We report here studies of post-transection changes in $[Na^+]_i$ in myelinated axons filled with SBFI, a ratiometric Na^+-sensitive dye. This technique allowed us to measure the spatiotemporal extent of the elevation of $[Na^+]_i$ around the injury site and to identify sites of functional membrane resealing. We also estimated the apparent rate of diffusion of Na^+ in the injured axon, and used these estimates to demonstrate that restoration of the normal low $[Na^+]_i$ occurs by a combination of passive redistribution and active extrusion, and that active extrusion can occur in an isolated internode. A preliminary report of this work has appeared (David, Barrett & Barrett, 1995*a*).

METHODS

Preparation and solutions

The experiments used large (up to 14 μm inner diameter) myelinated hypoglossal axons coursing along the thin ceratomandibularis muscle in small lizards (*Anolis sagrei*; see David, Modney, Scappaticci, Barrett & Barrett, 1995*b*). Lizards were killed by decerebration followed by destruction of the brain.

Preparations were bathed in a physiological salt solution (mM: 157 NaCl, 4 KCl, 2 $CaCl_2$, 2 $MgCl_2$), which contained in addition 5 mM glucose and 1 mM of a pH buffer (either Hepes or Pipes). Bath pH was maintained in the range 7·3–7·4, monitored using the indicator dye Phenol Red (5 mg l^{-1}). When the nerve was stimulated, muscle contractions were blocked with carbachol (150 μM). Unless otherwise specified, all reagents were from Sigma Chemical Co.; vanadate was purchased from Fisher Scientific Co. (Norcross, GA, USA). Muscle fibres on both sides of the main intramuscular nerve were cut parallel to the course of the nerve, producing a strip of muscle (~3 mm wide) which contained most of the nerve bundles innervating this preparation, coursing on or close to the ventral face of the muscle. The preparation was pinned ventral side down against a thin (No. 1) glass coverslip so that most axons lay within the working distances of the objectives used for fluorescent dye imaging (see below). A short (~0·5 mm) slit was cut in the muscle fibres covering the main intramuscular nerve bundle to allow impalement of visualized axons with dye-containing microelectrodes. All experiments were done at room temperature (20–25 °C).

Dye loading into axons

Microelectrodes for dye ionophoresis were pulled with a Brown-Flaming puller (Sutter Instrument Co.). Tips were back-filled with 5 mg ml^{-1} SBFI (tetra-ammonium salt, Molecular Probes) dissolved in water. Electrode barrels were filled with 3 M KCl. The resistances of filled electrodes ranged from 100 to 300 MΩ.

Axons were impaled using a piezoelectric device to 'tap' the microelectrode through the myelin sheath into the axon, as described in Barrett & Barrett (1982). Successful impalements were evidenced by recording a resting potential at least as hyperpolarized as −50 mV, and an action potential evoked by brief depolarizing pulses applied to the proximal nerve trunk via a suction electrode. These criteria were also used to ensure that the electrode tip remained intra-axonal throughout dye loading. SBFI was ionophoretically injected by applying continuous negative currents (0·5–5 nA) through the intra-axonal dye-filled electrode. Dye concentrations sufficient for reliable ratio measurements were typically achieved after 20–40 min of ionophoresis, and the electrode was then withdrawn from the axon.

Voltage recording and current passing and monitoring were done using a preamplifier (Axoclamp 2A, Axon Instruments) equipped with a bridge circuit. Signals were displayed on a digital oscilloscope (Tektronix 2212, Beaverton, OR, USA).

Axotomy

Single, dye-labelled axons were cut under visual control using a quartz microelectrode whose tip was broken to produce a cutting edge ~20–30 μm wide. The microelectrode was lowered onto the target axon using a hydraulic manipulator (Narashige, Tokyo, Japan) to press the axon against the glass coverslip. Axonal transection, verified by microscopic observation, was typically achieved within ~15–30 s, allowing dye imaging to resume within 1–2 min of transection. This transection site was 4–6 mm from the site where the nerve trunk was cut during the original dissection of the preparation.

Fluorescence measurements

Dye excitation. Excitation light came from an arc lamp source (Oriel, Stratford, CT, USA) equipped with a 1000 W Hg–Xe lamp. Fluctuations in light intensity were minimized using a photo-feedback system (Oriel) that maintained light intensity within 1% of the desired value. Spatial uniformity of light across the imaged fields was improved using ground quartz diffusers positioned after the main light source.

The excitation wavelengths required for SBFI ratio imaging (340 and 380 nm) were obtained by splitting the source light beam with a dichroic mirror at 360 nm, with the two light paths (wavelengths > 360 and < 360 nm) filtered by interference-type bandpass filters at 380 ± 20 and 340 ± 20 nm, respectively. The light path of the two beams was recombined using a dichroic mirror at 360 nm, and directed onto the preparation through the microscope objective. Switching between the two excitation wavelengths was achieved by alternately opening one of a pair of shutters positioned in the 340 and 380 nm light paths. All dichroic mirrors and filters were from Omega Optical Co. (Brattleboro, VT, USA). To minimize dye photo-bleaching and tissue damage, exposure times were limited to the periods of image acquisition, using an electromagnetically driven shutter on the light source.

Light collection. The preparation was imaged on the stage of a Reichert inverted microscope, equipped with ×40 (DApo 40UV/340, NA 1·30 oil, 160/0·17, working distance 0·22 mm) and ×20 (DApo 20UV/340, NA 0·65, 160/0·17, working distance 0·66 mm) objectives, both from Olympus. Light emitted in response to excitation of the indicator dye passed through a barrier filter (515 nm) and was captured with a cooled charge-coupled device (CCD) camera (CH-250, 16 bit, read-out rate 40 kHz, Photometrics, Tucson, AZ, USA). The light collection time, controlled with a 1 in Uniblitz shutter mounted in the camera, ranged from 20–200 ms in different experiments.

Image acquisition and storage. The opening and closing of the camera shutter, the light source shutter and the wavelength-switching shutters were co-ordinated using control pulses from a Tecmar A/D board installed in a 386 computer, using software written by Jim Gray (Department of Physiology and Biophysics, University of Miami). Each pair of images evoked by 340/380 nm excitation (500 × 500 pixels each) was acquired within < 0·5 s. The minimal inter-image interval of ~10 s was occupied mainly by storing these data to disk.

PMIS software (Photometrics) was used to transfer images to the memory of a 486 33 MHz computer. Images were saved on the hard disk and later transferred to an optical storage device (PMO-650, Pinnacle Micro, Irvine, CA, USA) for permanent storage and off-line analysis.

Fluorescence measurement and ratio calculation. Estimates of $[Na^+]_i$ were made using the ratio of the signals emitted by SBFI excited at 340 and 380 nm. During *in vivo* calibrations (see below) the 340 nm signal showed little change (less than 5%) and the 380 nm signal decreased when $[Na^+]$ increased, as also observed by Donoso, Mill, O'Neill & Eisner (1992) and Borzak *et al.* (1992) in rat cardiac myocytes. Intra-axonal dye concentrations fell following transection, but as long as dye signals remained detectable, the ratio of 340/380 nm signals could be used to measure $[Na^+]_i$. A

computer program (written in Pascal by G.D. and run on a Pentium computer) was used to correct for background fluorescence and then to calculate 340/380 nm emission ratios for various regions within the axon. With this program the user defines various rectangular intra-axonal regions of interest (ROI) along the length of the dye-injected axon (see rectangles labelled *a–d* in Fig. 2*A*). Each intra-axonal ROI was matched with a nearby background region (not shown) defined in a dye-free region of the field just outside the 'flare' surrounding the dye-filled axon. For a given intra-axonal ROI the ratio $R_{340/380}$ was computed as (mean 340 nm signal within ROI − mean 340 nm signal in matched background region)/(mean 380 nm signal within ROI − mean 380 nm signal in matched background region). Changes in $R_{340/380}$ for up to eight ROIs within a given axon were measured in the resting axon and at various times after transection. If the axon changed its position within the image field, as usually occurred after axotomy, the ROIs were repositioned as close as possible to their original intra-axonal locations, using visible morphological landmarks such as nodes of Ranvier and clefts of Schmidt–Lanterman. If images within a given 340/380 nm pair shifted relative to each other (a rare event), that image pair was discarded from the analysis. $R_{340/380}$ values were plotted *vs.* time and/or distance along the axon using Coplot (CoHort Software, Berkeley, CA, USA). Most observations were made on the proximal (i.e. nearer the spinal cord) side of the transection.

Dye calibration. Intra-cytoplasmic calibration of the SBFI emission ratio requires permeabilization of the cell membrane with a Na^+ ionophore, but in the large-diameter axons imaged here, the myelin sheath restricts access of both ionophore and changes in bath [Na^+] to the internodal axolemma. We were able to obtain some calibration data from regions of axon more accessible to the bath, namely small axonal branches and their attached motor terminals (Fig. 1), but these preparations required such long equilibration times (15–60 min) that it was difficult to complete the entire calibration curve in a single preparation. Thus Fig. 1 includes, for comparison, similar calibration curves obtained in a more tractable preparation (cultured rat neurones), whose physiological saline has an ionic strength similar to that of lizards. These neurones were obtained from embryonic day 15 septum plated on polylysine-coated glass coverslips, and maintained in culture for 2 weeks using techniques described in Nonner, Brass, Barrett & Barrett (1993). Large neurones were filled with SBFI using ionophoretic techniques similar to those described above for lizard axons, except that shorter injection times sufficed to fill the neurones with dye.

To facilitate transmembrane equilibration of Na^+ and K^+, calibration solutions contained the ionophores gramicidin D (3 μM) and monensin (10 μM) and the Na^+,K^+-ATPase inhibitor ouabain (1 mM). Calibration solutions contained 10 mM Hepes, pH 7·3, and solutions used with axons also contained 20 μM veratridine to block inactivation of depolarization-activated Na^+ channels. Following 20–30 min exposure to the ionophores and ouabain, SBFI-filled cells were imaged in a series of bathing solutions in which Na^+ was lowered by replacement with K^+ to achieve bath [Na^+] spanning the range 0 to 160 mM (Na^+ plus K^+ = 160 mM). This K^+ for Na^+ substitution is appropriate for this study, since Na^+ entering an injured axon would be expected to displace a roughly equivalent amount of K^+. We also tested solutions in which total bath [Na^+] was increased to 200 mM (see description of Fig. 2).

Figure 1 plots measured 340/380 nm ratios as a function of both total bath [Na^+] (upper abscissa) and Na^+ activity (lower abscissa). Na^+ activity was calculated using activity coefficients listed in Robinson & Stokes (1959) for different total NaCl concentrations. Calibrations were similar in axonal branches and neurones, and when chloride, sulphate or gluconate was the major bath anion. A caveat is that, because the imaged axon branches and terminals remained attached to the parent axon, we could not be certain that $[Na^+]_i$ was truly zero in axon branches and terminals exposed to the 0 Na^+ calibrating solution. This problem might cause us to underestimate the resting $[Na^+]_i$. Another caveat is that it was not possible to control pH in myelinated axons. Like Rose & Ransom (1996), we found that the SBFI 340/380 nm ratio decreased as the pH was made more acidic. For a bath [Na^+] of 80 mM, changing the pH from 7·3 to 6·8 reduced the 340/380 nm ratio as much as a 6–8 mM reduction in bath [Na^+] (not shown). Small errors due to changing pH would not alter the major conclusions of this study.

Interpolation between measured calibration points used an equation adapted from eqn (4) in Donoso *et al.* (1992):

$$R = R_0([Na^+] + K_d)/([Na^+] + K_d + \beta[Na^+]R_0), \quad (1)$$

where R is the 340/380 nm fluorescence ratio measured as described above, and R_0 is the ratio measured when bath [Na^+] = 0 mM. A value of 29 mM for K_d, the apparent dissociation constant of SBFI for Na^+, was obtained from a Hanes plot (not shown) of $[Na^+]_o/(1/R_0 - 1/R)$ *versus* $[Na^+]_o$, as described in Donoso *et al.* (1992). Using this K_d eqn (1) was fitted to the calibration data (least mean square method, CoStat software in Coplot), yielding a value

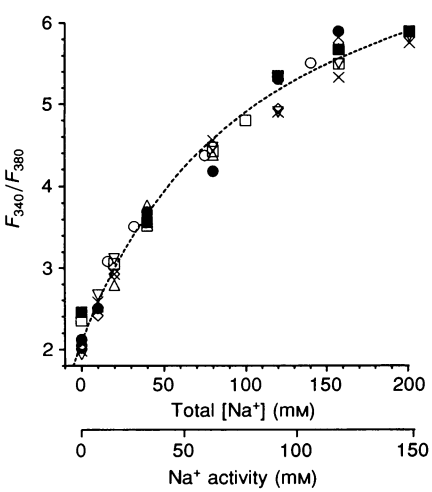

Figure 1. Calibration curve relating SBFI 340/380 nm emission ratio to total bath [Na^+] (upper abscissa) and Na^+ activity (lower abscissa)
Filled symbols plot ratios measured in juxta-terminal axon (circles) or motor terminal boutons (squares). All other symbols came from cultured septal neurones, each symbol representing a different preparation. Measured points were fitted with the indicated curve using an equation in the text derived from Donoso *et al.* (1992). For total [Na^+] < 160 mM, K^+ was added to maintain osmolarity. Most solutions incorporated the 30 mM Cl^-–110 mM gluconate anion mixture described by Harootunian, Kao, Eckert & Tsien (1989) to minimize cell swelling. In other cases the bath anion was Cl^- (diamonds) or a mixture of sulphate and Cl^- (open circles and inverted triangles). Other components of the calibration solutions are described in Methods. Na^+ activity calculations used values reported for NaCl; our measurements of osmolarity suggested that the dissociation of sodium gluconate is about 4% less than that of NaCl in 160 mM solutions.

of −0·355 for the constant β (dashed line, Fig. 1). A rearranged form of eqn (1):

$$[Na^+]_i = K_d(R_0 - R)/(R(1 + \beta R_0) - R_0),$$

was used to convert R values measured in axons to $[Na^+]_i$.

The 29 mM apparent K_d for SBFI in these cells is higher than the value of 17 mM measured in mixed Na^+–K^+ solutions *in vitro* by Minta & Tsien (1989), but is identical to that measured by Donoso *et al.* (1992) in rat ventricular myocytes.

Measurements reported here came from axons in which the resting 340/380 nm ratio was stable for at least 15 min. In such axons the emissions ratio indicated a resting $[Na^+]_i$ in the range 5–15 mM.

RESULTS

Changes in $[Na^+]_i$ following axonal transection in physiological saline

Figure 2 depicts an experiment in which an SBFI-loaded axon was transected in normal lizard saline. Panel *A* shows pseudocolour ratio images of the axon along with a diagram obtained by tracing a phase image (not shown). Dotted lines indicate the site of transection. The pseudocolour images show a low ratio throughout the axon before transection and a uniformly high ratio 1 min after transection, with recovery of the control ratio in part of the axon 116 min after transection. The labels *a*–*d* indicate four regions

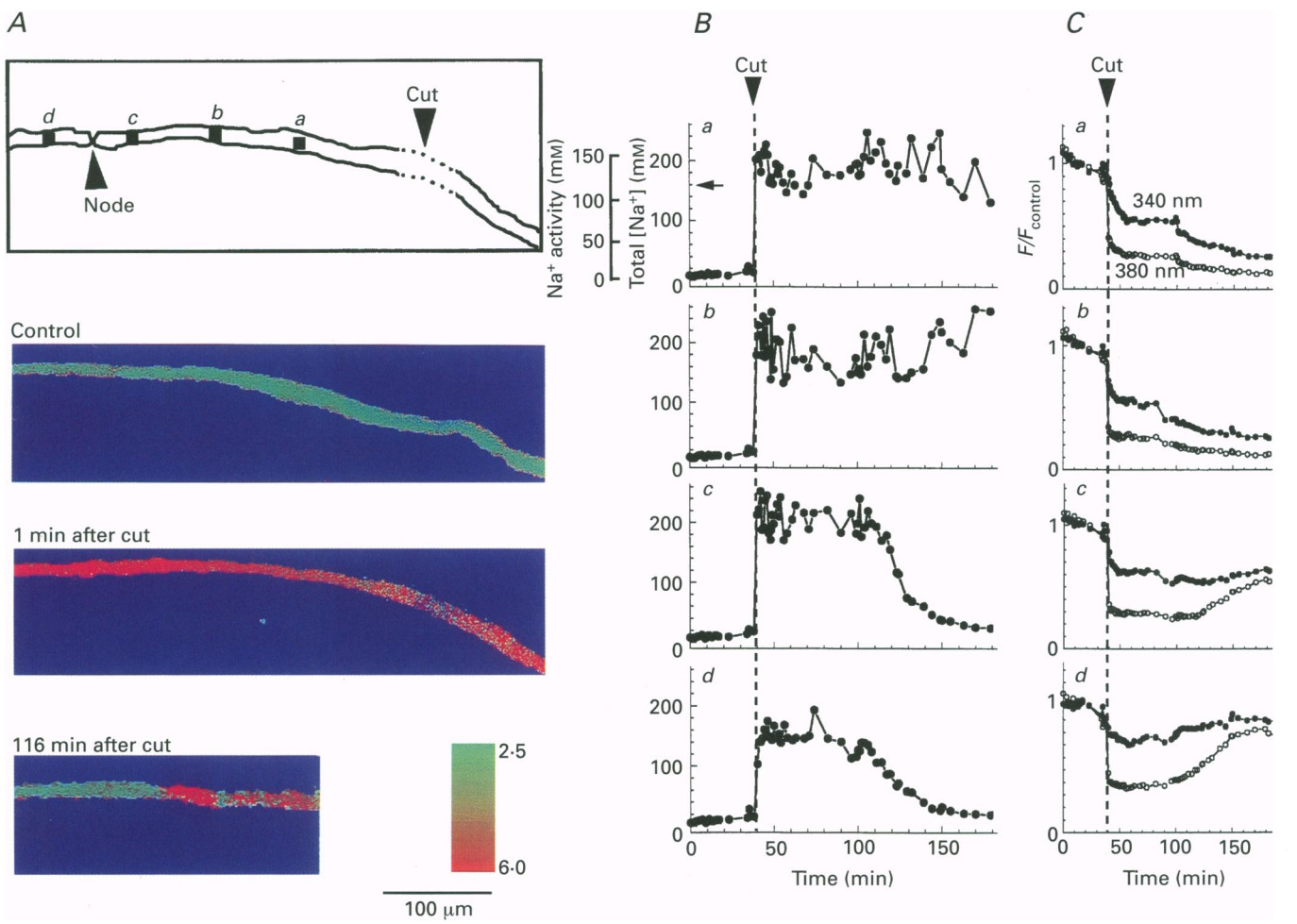

Figure 2. Spatial and temporal changes in fluorescent emissions and $[Na^+]_i$ following transection of an SBFI-injected axon

A, pseudocolour images of the 340/380 nm emission ratio taken before (control) and 1 and 116 min after transection at the site indicated in the line drawing. Higher ratios (red colour) indicate higher $[Na^+]_i$ (see colour calibration bar). At 116 min after transection no signal was detected between the region labelled *a* and the cut, presumably due to loss of dye out of the cut end. *B*, time course of changes in $[Na^+]_i$ at regions *a*, *b*, *c* and *d* labelled in *A*, obtained from 340/380 nm emission ratios using the calibration curve in Fig. 1. Separate ordinates plot total $[Na^+]$ and estimated Na^+ activity; arrow in the upper record indicates bath $[Na^+]$. *C*, time course of changes in fluorescent emissions evoked by excitation with 340 (●) and 380 nm (○) light in regions *a*–*d*. Fluorescence values (corrected for background) were normalized to the average pre-transection fluorescence for that wavelength and region ($F/F_{control}$). Axis labels in *Ba* and *Ca* are applicable to all panels.

within the axoplasm (separated from each other by 80 μm) whose normalized, averaged fluorescent emissions following excitation at 340 and 380 nm are plotted in panel *C*. Panel *B* shows the time course of changes in $[Na^+]_i$ calculated for regions *a–d*.

After transection $[Na^+]_i$ increased rapidly to concentrations approaching or exceeding those in the bath over the entire sampled length of axon (up to ~400 μm from the transection site), and remained at these high levels for many minutes. Both 340 and 380 nm signals decreased following transection; reduction of the 340 nm signal, which was relatively insensitive to changes in $[Na^+]$ during intracellular calibration, indicates loss of dye out of the cut end. The finding that post-transection $[Na^+]_i$ often exceeded bath $[Na^+]$ was surprising at first, but consideration of the electrical forces acting on Na^+, the restriction of axonal swelling imposed by the myelin and connective tissue surrounding the axon, and analysis of published data from X-ray microprobe studies of injured myelinated axons suggests that these high measured $[Na^+]_i$ values are real rather than artifactual (see Discussion).

$[Na^+]_i$ subsequently recovered its low resting value at sites distant from the transection; this decrease began ~65 min after transection in region *d*, and ~80 min after transection in region *c* in Fig. 2. In regions closer to the transection site (*a* and *b*) $[Na^+]_i$ remained high, and at later times became quite variable due to loss of signal resulting from continued leakage of dye out the cut end.

The pseudocolour ratio image computed 116 min after transection shows a sharp gradient in the 340/380 nm ratio ~200 μm from the cut end (between regions *b* and *c*). We hypothesize that this gradient represents a site of functional membrane resealing, separating the proximal region of the axon where $[Na^+]_i$ recovered from the distal region nearer the transection where $[Na^+]_i$ did not recover. Consistent with this hypothesis, at late times the normalized fluorescence ($F/F_{control}$) plots in Fig. 2*C* showed a continuing reduction in the 340 nm signal in regions *a* and *b* (suggesting continued loss of dye), whereas in regions *c* and *d* the 340 nm signal rose as the 340/380 nm ratio (and thus $[Na^+]_i$) started to fall, suggesting replenishment of dye by diffusion from more proximal (uninjured) regions of the axon. Thus defined, membrane resealing occurred between 6 and 55 min after transection at sites 50–320 μm from the transection in a sample of ten axons (means ± S.D.: 20 ± 15 min, 160 ± 85 μm). In three of these axons there was a node within the microscope field (e.g. diagram in Fig. 2), and in one of these axons the node was the resealing site. Over the lengths of proximal axon we observed, restoration of the resting $[Na^+]_i$ following a single transection was complete within 40–70 min.

Although the major functional resealing site for the axon of Fig. 2 was between regions *b* and *c*, there were suggestions that resealing-related events also occurred closer to the transection site. Sometimes this distal region showed alternating regions with and without dye signals, suggesting

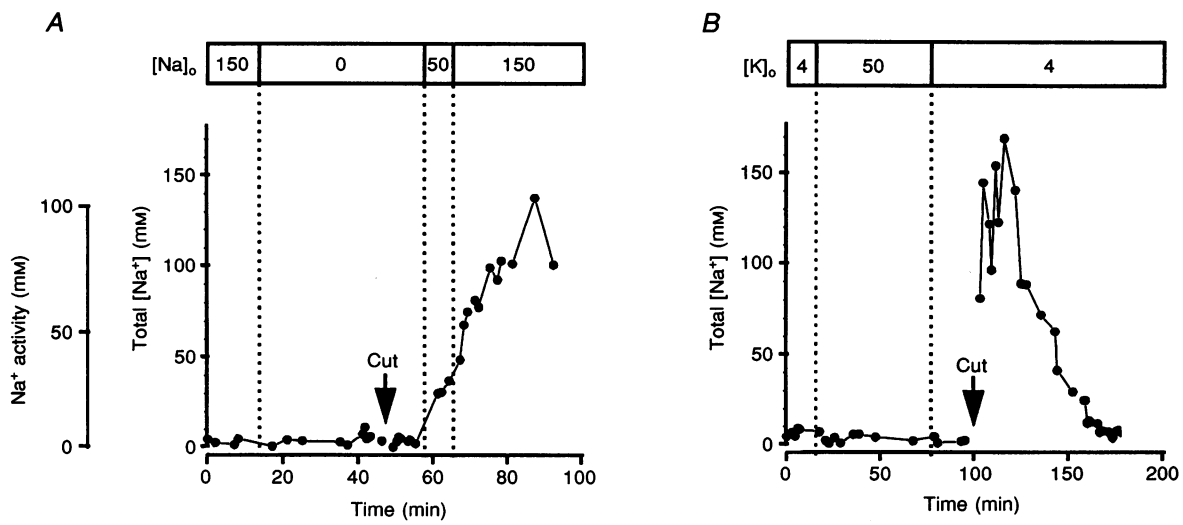

Figure 3. Evidence that the post-transection increase in $[Na^+]_i$ was due mainly to Na^+ entry through the transection site

A, $[Na^+]_i$ in an axon transected in the absence of bath Na^+ and later re-exposed to Na^+. The solution containing 150 mM Na^+ also contained 50 mM K^+, the zero Na^+ solution contained 150 mM choline and 50 mM K^+, and the 50 mM Na^+ solution also contained 150 mM choline (all as chloride salts). Following transection $[Na^+]_i$ did not rise until Na^+ was restored to the bath. *B*, depolarizing another axon by elevating bath $[K^+]$ from the normal 4 mM to 50 mM (by addition of K_2SO_4) produced no discernable increase in $[Na^+]_i$, although this axon subsequently showed a large post-transection increase in $[Na^+]_i$. Axons in *A* and *B* were imaged in regions ~110 and ~170 μm from the cut, and showed evidence of functional resealing (not shown) at ~25 and ~20 min after the cut at distances ~320 and ~170 μm from the cut, respectively.

the alternating regions of axonal swelling and constriction (beading) associated with transection sites (e.g. Xie & Barrett, 1991). Also, the rate of decrease of the 340 nm signal changed following transection, from the rapid decrease seen immediately after transection to the almost constant levels seen during the late phase of the high $[Na^+]_i$ plateau 10–40 min after transection. Some slowing of the rate of decrease of the 340 nm signal would be expected simply from reduction in the concentration gradient driving diffusion of dye out of the cut end of the axon, but some slowing may also have been due to constriction of the axon occurring even before $[Na^+]_i$ began to decrease in proximal regions. Another possible explanation is a reduction in the magnitude of the injury current, since this current would tend to ionophorese dye out of the axon.

Thus our measurements of the site of functional membrane resealing based on development of a sharp intra-axonal $[Na^+]$ gradient do not measure the only site of resealing-related events, but rather the resealing site that remained in continuity with the parent axon. Likewise, the time at which this intra-axonal $[Na^+]$ gradient developed does not measure the onset of resealing-related events, but rather the time when resealing was sufficiently complete to permit Na^+ efflux from the imaged region (by, for example, active transport as well as diffusional redistribution of Na^+ into the

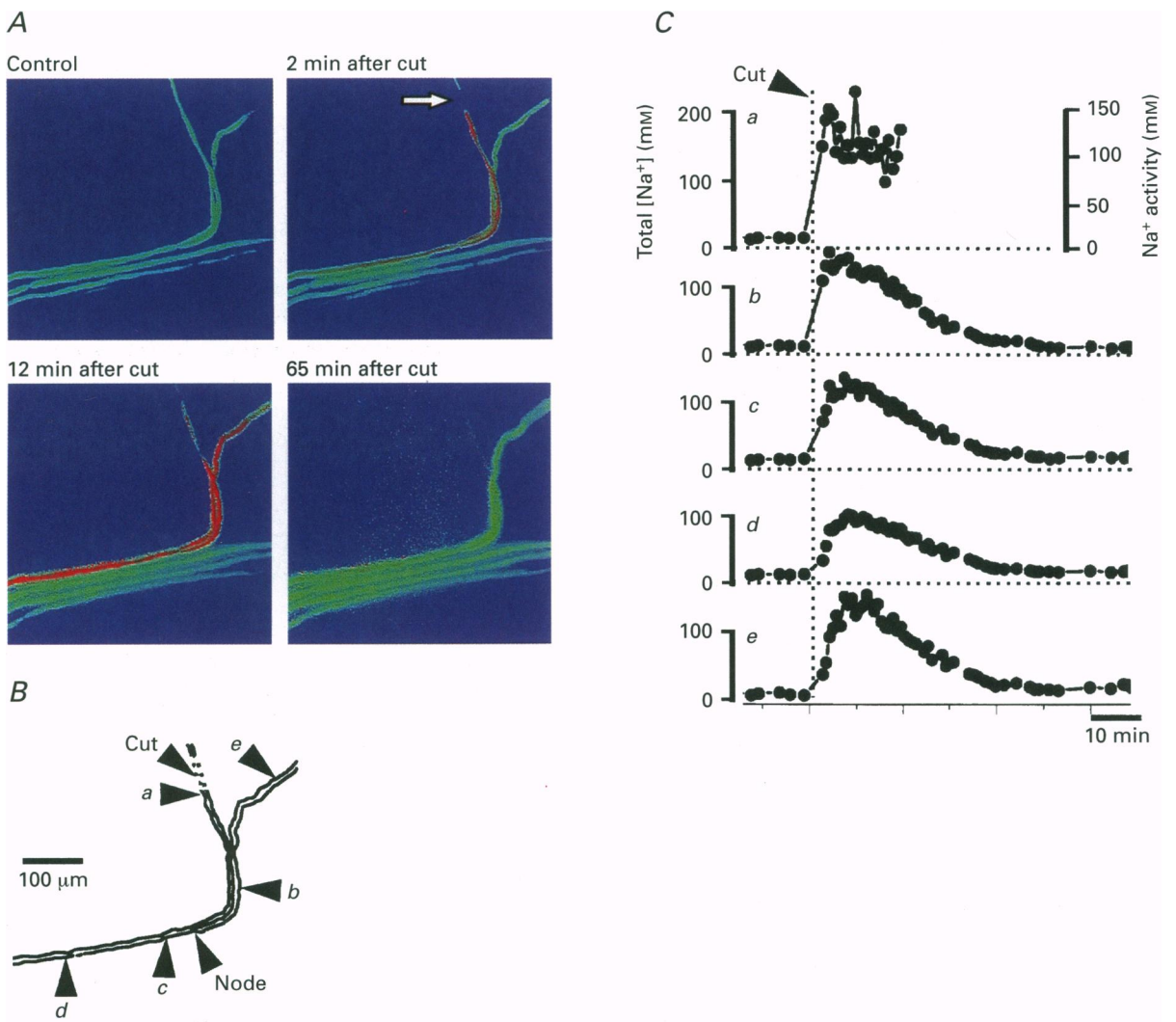

Figure 4. Bidirectional spread of Na^+ in a transected axon

Pseudocolour images show 340/380 nm emission ratios before and at 2, 12 and 65 min (*A*) after transection of one branch of the axon shown in the diagram (*B*). (Three additional SBFI-injected axons which were not cut showed no significant changes in $[Na^+]_i$ over the course of the experiment.) Graphs in *C* plot changes in $[Na^+]_i$ for regions on the cut branch (*a* and *b* in diagram), the parent axon (*c* and *d*), and a non-transected branch (*e*), illustrating that the $[Na^+]_i$ elevation spread in both proximal and distal directions along the injured axon. $[Na^+]_i$ could not be determined at region *a* at later times due to loss of dye out of the cut end. Axis labels in panel *Ca* are applicable to all panels.

proximal axon) to begin to exceed the injury-associated Na^+ influx.

The post-transection increase in $[Na^+]_i$ is dominated by entry of Na^+ from the bath into the cut end of the axon

Figure 3 provides further evidence that the increase in $[Na^+]_i$ following transection was due to Na^+ entry through the cut end. In panel *A* an SBFI-filled axon transected in Na^+-free solution and imaged at a site 110 μm from the transection showed no detectable increase in $[Na^+]_i$ over a 10 min interval. (Other axons transected in normal bath $[Na^+]$ and imaged at a similar distance from the transection site always showed an increase of at least 100 mM in $[Na^+]_i$ during this time.) Subsequent elevation of bath $[Na^+]$ to 50 and then 150 mM was followed by a ~140 mM increase in $[Na^+]_i$, indicating that the source for the post-transection increase in $[Na^+]_i$ was Na^+ from the bathing solution.

Na^+ might enter axons through the transection site and/or through Na^+ channels activated by transection-induced depolarization. Figure 3*B* shows that depolarization *per se* (with 50 mM bath $[K^+]$) for ~1 h produced no detectable change in $[Na^+]_i$, whereas subsequent transection of the axon in physiological saline caused the expected rapid elevation in $[Na^+]_i$. The absence of any detectable sustained increase in $[Na^+]_i$ in 50 mM K^+ was consistent ($n = 3$), and is not surprising, since most depolarization-activated Na^+ channels in large axons inactivate during maintained depolarization, and extrusion of any entering Na^+ by axolemmal Na^+,K^+-ATPase would be facilitated by the high bath $[K^+]$. $[Na^+]_i$ did increase in high bath $[K^+]$ if Na^+ channel inactivation was inhibited by addition of 20 μM veratridine ($n = 2$, not shown). The experiment of Fig. 6, which was performed in the presence of 5 μM tetrodotoxin (TTX), shows that the rapid post-transection increase in $[Na^+]_i$ did not require Na^+ entry via TTX-sensitive channels. These findings suggest that most of the measured post-transection increase in $[Na^+]_i$ was due to Na^+ entry at the transection site.

Spatiotemporal gradients of $[Na^+]_i$ along the transected axon

If Na^+ entering via the cut end spreads along the axon by diffusion, then one would expect $[Na^+]_i$ to be elevated both proximal and distal to the cut end, as was indeed seen in the pseudocolour image at 1 min in Fig. 2*A*. The experiment in Fig. 4 illustrates more clearly that the $[Na^+]_i$ elevation spread in both distal-to-proximal and proximal-to-distal directions. Here one of two axonal branches was transected, and computed transients showed that the rapid increase in $[Na^+]_i$ spread from the cut branch (regions *a* and *b*) into both the parent axon (regions *c* and *d*) and the uncut branch (region *e*) via the intervening node.

To examine in a more quantitative manner whether the initial increase in $[Na^+]_i$ after transection could be accounted for by diffusion, we used the diffusion equation for a semi-infinite medium in which the boundary is kept at a constant $[Na^+]$ (Crank, 1975, pp. 20–21, eqn 2·45):

$$C_{in}/C_{out} = \mathrm{erfc}[X/(4Dt)^{0.5}], \quad (2)$$

where C_{in} and C_{out} are (respectively) the intra-axonal and bath concentrations of Na^+, erfc is the complementary error function, X is the distance from the boundary (cut end), D is the apparent diffusion coefficient for Na^+ in the axoplasm, and t is time after transection. Rearrangement of eqn (2) gives:

$$\mathrm{erfc}^{(-1)}(C_{in}/C_{out}) = (X/t^{0.5})(1/(4D)^{0.5}). \quad (3)$$

Thus if the spread of Na^+ along the transected axon occurs by simple diffusion, a plot of $\mathrm{erfc}^{(-1)}(C_{in}/C_{out})$ against $X/t^{0.5}$ should yield a straight line with a slope of $1/(4D)^{0.5}$, enabling estimation of the apparent diffusion coefficient for Na^+ within transected axons. Figure 5 shows data from three transection experiments plotted in this way. The correlation coefficient (R) was 0·77, S.E.M. = 0·052, with P for the correlation < 0·0001. From the slope of the line fitted to these experimental points the apparent diffusion coefficient for Na^+ within the transected axon was calculated to be

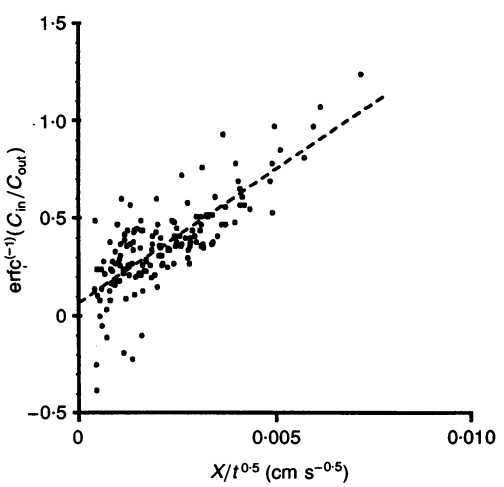

Figure 5. Estimate of apparent diffusion coefficient (D) for Na^+ in the axoplasm of transected axons

The inverse of the complementary error function ($\mathrm{erfc}^{(-1)}$) of the ratio of intracellular to extracellular $[Na^+]$, (C_{in}/C_{out}), is plotted as a function of distance from the cut divided by the square root of the time after the cut. Points were obtained from measurements of $[Na^+]_i$ in 3 SBFI-filled axons transected in control saline, and were limited to regions containing sufficient SBFI to permit reliable measurements of 340/380 nm ratios, and to times prior to functional resealing. Times ranged from 1·3 to 14·7 min after the cut and distances ranged from 90 to 630 μm (median 285 μm) from the cut. The dashed line fitted to these data had a correlation coefficient of 0·77. As described in the text, the slope of this line should equal $1/(4D)^{0.5}$, yielding $D = 1{\cdot}33 \times 10^{-5}$ cm^2 s^{-1}.

$1{\cdot}33 \times 10^{-5}$ cm^2 s^{-1} (upper and lower 95% confidence limits $1{\cdot}78 \times 10^{-5}$ and $1{\cdot}03 \times 10^{-5}$ cm^2 s^{-1}, respectively). This value is an apparent, rather than a true, diffusion coefficient, because Na^+ movements within the transected axon were probably influenced by electrical as well as concentration gradients (see Discussion).

Recovery of $[Na^+]_i$ cannot be accounted for by diffusional redistribution alone

When the axonal membrane reseals, thus reducing influx of Na^+, recovery of $[Na^+]_i$ towards its low resting level at locations proximal to the resealing site might occur via both passive and active mechanisms. The passive mechanism is redistribution of Na^+ within the resealed axon, from regions near the resealing site to more proximal regions of the axon that have not lost their transmembrane $[Na^+]$ gradient. If the total length of the resealed axon were long enough, it is possible that such passive redistribution could reduce $[Na^+]_i$ to levels close to pre-transection levels. The most likely active mechanism for reducing $[Na^+]_i$ is Na^+ extrusion by the electrogenic Na^+,K^+-ATPase. Consistent with the presence of such a pump, these lizard axons exhibit a post-tetanic hyperpolarization that is inhibited by ouabain, by removal of extracellular K^+, and by replacement of bath Na^+ with Li^+ (Morita, David, Barrett & Barrett, 1993).

Figure 6 illustrates an experiment testing the extent to which passive redistribution can account for recovery of $[Na^+]_i$ in transected axons. As shown in the diagram, this axon was transected at one site and then 80 min later was transected again at a more proximal site within the same internode. The pseudocolour images show large increases in the 340/380 nm ratio throughout the imaged region after each transection (*b* and *d*), with nearly complete recovery

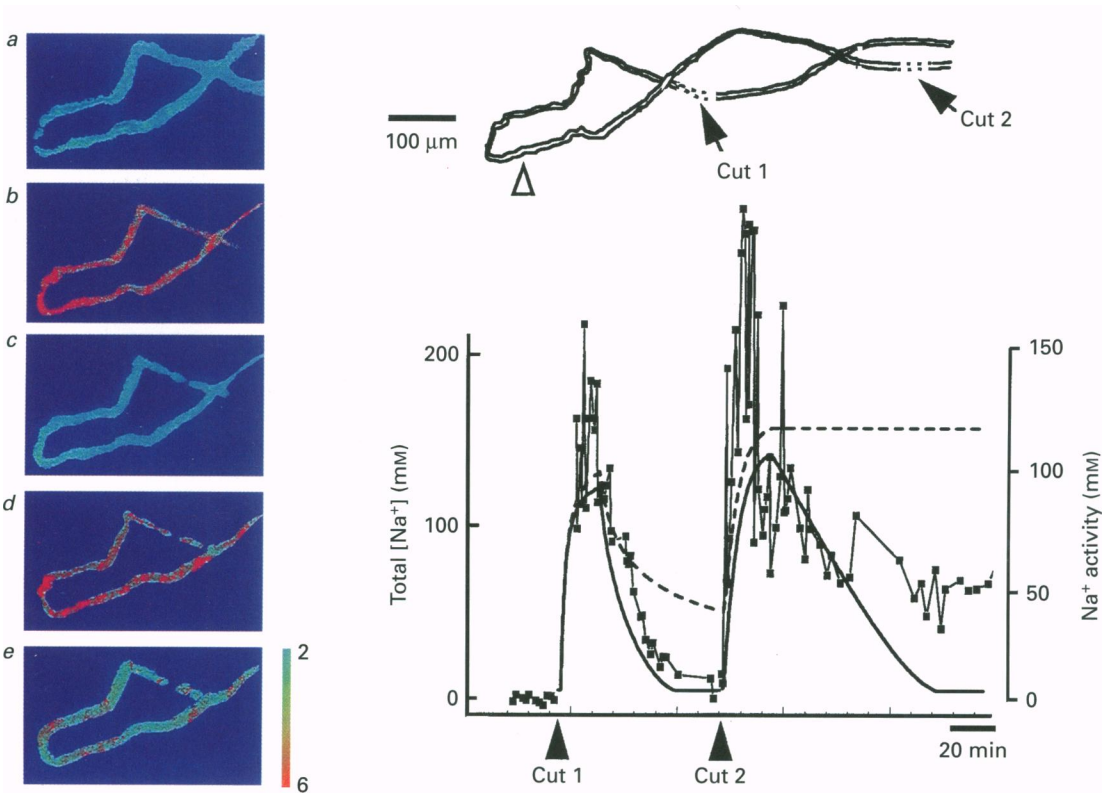

Figure 6. Changes in $[Na^+]_i$ following sequential transections (cut 1 and 2 in diagram)

The second transection occurred ~80 min after the first at a site more than 1 mm distant, but still within the same internode. Pseudocolour images show 340/380 nm ratios before transections (*a*), 5 and 71 min after the first transection (*b* and *c*), and 2 and 110 min after the second transection (*d* and *e*), respectively. In the graph the points connected by thin continuous lines plot the time course of changes in $[Na^+]_i$ in the region indicated by the open arrowhead in the diagram. The nerve trunk containing this axon was folded to allow the entire axonal length between the cuts to be imaged within the same microscope field. Tetrodotoxin (5 µM) was present throughout. The dashed curve predicts changes in $[Na^+]_i$ based on diffusion alone, and the continuous curve predicts the combined effects of diffusion and active pumping. Simulations assumed an $[Na^+]_i$ of 5 mM in the uninjured axon and an axonal radius of 5 µm, and divided the measured 6 mm length of this axon proximal to the first transection (only ~1 mm of which is visible in the diagram) into 200 slices each 30 µm long. We assumed that the cut end remained open to the bath as long as $[Na^+]_i$ was rising; the location and time of resealing were matched to those estimated for this axon from measurements of $[Na^+]_i$. Pump activity, calculated using the equation given in the text, was terminated when $[Na^+]_i$ was restored to its resting level of 5 mM.

71 min after the first transection (compare *c* with pre-transection *a*), and partial recovery in the axonal segment isolated by the second transection (compare *e* with *c*). In the graph the points connected by thin lines plot $[Na^+]_i$ measured in a region midway between the two transections, illustrating the slower, incomplete restoration of $[Na^+]_i$ following the second transection.

The dashed curve in Fig. 6 shows changes in $[Na^+]_i$ predicted assuming passive diffusion of Na^+ into the axon and passive redistribution of intra-axonal $[Na^+]_i$ following resealing. Transections were simulated in a multi-compartmental computer model by removing a diffusion barrier for Na^+ at one end of the model axon, allowing bath Na^+ to diffuse into the axon with the apparent Na^+ diffusion coefficient estimated in Fig. 5. Membrane resealing was simulated by restoring this diffusion barrier at the time when the measured $[Na^+]_i$ began to fall (see legend for further details concerning simulation). This passive model predicted partial recovery of $[Na^+]_i$ after the first transection, but no recovery within the segment isolated by the second transection. After each transection the observed recovery of $[Na^+]_i$ was more complete than that predicted by passive redistribution, suggesting that active mechanisms contributed to the observed post-transection restoration of $[Na^+]_i$. The axon segment isolated by the transections contained no visible node, so it appears that internodal axonal membranes can actively extrude Na^+. $[Na^+]_i$ usually failed to recover in isolated axonal segments less than 0·5 mm long (not shown).

The continuous curve in Fig. 6 shows changes in $[Na^+]_i$ predicted by adding an active pump to the passive redistribution model described above. Pump activity, assumed to be uniformly distributed along the axon and to have Michaelis–Menten kinetics, was simulated using the equation:

$$C_{t+\Delta t} = -V_{max} A \Delta t C_t / V(C_t + K_m),$$

where C is $[Na^+]_i$ at time t, V_{max} is the maximal pump rate (see below), A is the area of axonal membrane, V is the volume of the intra-axonal compartment, and K_m is the dissociation constant of the pump, assumed to be 15 mM (McGill, 1991). The maximal pump rate that best fitted the data was 1×10^{-9} mM cm^{-2} s^{-1}, which falls at the low end of pump rates calculated from the rates of Na^+ extrusion estimated in Morita *et al.* (1993) from the post-tetanic hyperpolarization measured in these axons. These simulations thus suggest that pump activity plus diffusional redistribution were sufficient to account for the observed rate of recovery of $[Na^+]_i$.

In an attempt to demonstrate more directly the contribution of active processes to post-transection recovery of $[Na^+]_i$, we transected axons in the presence of 1–2 mM vanadate and/or 1 mM ouabain, which inhibit Na^+,K^+-ATPase activity from intracellular and extracellular sites, respectively. In two experiments (not shown) these inhibitors made no detectable difference in the timing of resealing or the rate of $[Na^+]_i$ restoration following the first transection, but did abolish $[Na^+]_i$ recovery in segments $\geqslant 1$ mm in length isolated by a second transection, in which partial recovery of $[Na^+]_i$ would normally occur (Fig. 6). We suspect that the failure of vanadate and ouabain to inhibit $[Na^+]_i$ recovery following the first transection was attributable to at least two factors. First, diffusional redistribution of Na^+ (which would not be blocked by vanadate or ouabain) makes a large contribution to the decrease in $[Na^+]_i$ observed following the first transection. Second, both inhibitors probably had restricted access to pump sites in the internodal axolemma. Bath-applied ouabain can reach pump sites at nodes and terminals fairly rapidly (Morita *et al.* 1993), but probably requires longer times to reach the internodal axolemma. The access of bath-applied vanadate to the interior of the lesioned axon would be reduced by injury currents, which would retard entry of anions.

Experiments like those in Fig. 6 suggested that the internodal axolemma can actively extrude Na^+. Since in the intact axon most Na^+ entry occurs at the node, and most immunohistochemically detected Na^+,K^+-ATPase is localized at nodes (reviewed in Sweadner, 1989), we wondered whether internodal pumps would ever be activated in the intact axon. Figure 7 shows that internodal $[Na^+]_i$ did indeed increase during stimulation, although intense, prolonged stimulation (50 Hz for at least 2 min) was

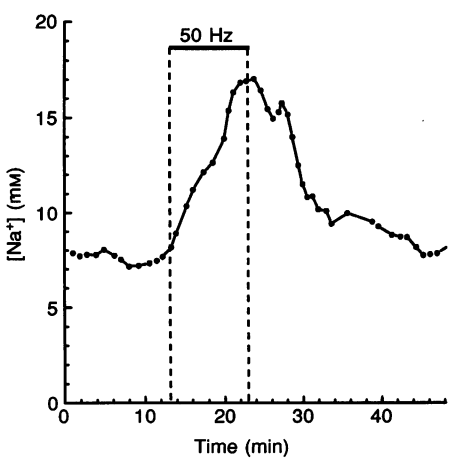

Figure 7. Reversible increase in $[Na^+]_i$ produced by 50 Hz stimulation of the proximal nerve trunk
Dashed lines indicate duration of stimulation.

required to produce a detectable increase ($n = 2$). This result suggests that internodal pumps may be activated during intense stimulation.

DISCUSSION

Results presented here provide the first measurements of the spatial and temporal profile of the rise and fall of $[Na^+]_i$ that occurs in vertebrate myelinated axons in response to transection. These results also offer a novel technique for estimating the timing and location of functional resealing of the axon membrane.

Na^+ entry into transected axons

Following transection $[Na^+]_i$ near the cut end rose rapidly to levels that frequently exceeded that in the bath. We hypothesize that these high $[Na^+]_i$ levels arose from massive Na^+ influx through the cut end, overwhelming the ability of the pump to extrude Na^+, combined with Gibbs–Donnan and electrical forces attracting Na^+ into the injured axon, and constraints on axonal swelling imposed by the surrounding myelin sheath and connective tissue. With respect to the Gibbs–Donnan forces exerted by non-diffusible intracellular anions, one can calculate (assuming 155 mM Na^+ in the bath) that a Na^+-permeable cell containing 75 mequiv of non-diffusible anionic charge would at equilibrium contain 200 mM Na^+, as measured in some transected axons (Figs 2, 4 and 6). With respect to electrical gradients, the axon near the cut end is likely to have a small negative transmembrane potential due to its connection to more proximal regions of the axon, where K^+ efflux via non-inactivating delayed rectifier and Na^+-activated K^+ channels (Koh, Jonas & Vogel, 1994; Poulter, Hashiguchi & Padjen, 1995) would be expected to be increased. A membrane potential as low as -6 to -7 mV in a Na^+-permeable cell would predict a steady-state $[Na^+]_i$ of 200 mM (assuming 155 mM bath $[Na^+]$). The Na^+ influx associated with mechanical injury osmotically induces an accompanying water influx and cell swelling. In cells with unlimited capacity for expansion such water influx would largely offset increases in $[Na^+]_i$; the cell would simply swell until it burst or until it recovered sufficiently to start pumping out the accumulated Na^+. However, the myelin sheath and connective tissue surrounding these axons would be expected to limit the extent to which the injured axon can swell (Rand, Fuller & Lis, 1979), permitting the development of $[Na^+]_i$ exceeding that in the bath.

$[Na^+]_i$ in excess of bath values can also be calculated from X-ray microprobe measurements of anoxic rat optic nerve axons reported by LoPachin & Stys (1995). These authors reported their Na^+ measurements with respect to dry weight, but when these values are corrected for axonal water content and an estimated intracellular Na^+ activity coefficient, more than 10% of axons subjected to 1 h of anoxia followed by 1 h reoxygenation exhibited $[Na^+]_i$ exceeding bath levels (P. Stys, personal communication). These findings support the hypothesis that $[Na^+]_i$ in injured axons can indeed reach levels exceeding bath $[Na^+]$.

The post-transection increase of $[Na^+]_i$ required the presence of Na^+ in the bathing solution, but did not require TTX-sensitive Na^+ channels. Measurements summarized in Fig. 5 indicate that the spread of $[Na^+]_i$ within injured axons could be reasonably well described by simple diffusion from the cut end. Injury currents would also facilitate Na^+ influx into the transected axon. Another possible route of Na^+ entry is via Na^+–Ca^{2+}exchangers. Immunocytochemical evidence from rat neuromuscular preparations suggests that one exchanger isoform is present primarily in motor nerve terminals rather than in myelinated regions of peripheral axolemma (Luther, Yip, Bloch, Ambesi, Lindenmayer & Blaustein, 1992), but mRNA encoding an additional exchanger isoform has been detected in rat spinal motoneurones (Marlier, Zheng, Tang & Grayson, 1993), and Lehning, Doshi, Isaksson, Stys & LoPachin (1996) present evidence compatible with the hypothesis that reversed operation of a Na^+–Ca^{2+} exchanger contributes to Ca^{2+} entry in anoxic rat peripheral nerve.

We computed an apparent diffusion coefficient for Na^+ in transected axons ($1{\cdot}33 \times 10^{-5}$ cm^2 s^{-1}, Fig. 5) to allow us to estimate the effect of passive redistribution on the time course of recovery of $[Na^+]_i$ following transection and resealing. This apparent diffusion coefficient is similar to diffusion coefficients measured for Na^+ in free solution ($1{\cdot}32 \times 10^{-5}$ cm^2 s^{-1}, Wang, 1952; $1{\cdot}48 \times 10^{-5}$ cm^2 s^{-1}, Robinson & Stokes, 1959). Measurements of Hodgkin & Keynes (1956) in Na^+-injected squid axons and of Lasser-Ross & Ross (1992) in SBFI-injected rat Purkinje neurones are also compatible with rapid diffusion of Na^+ within neuronal cytoplasm. However, the measurement by Hinke (1961) of Na^+ activity in squid axons suggested that 24% of intra-axonal Na^+ is bound. Also, Kushmerick & Podolsky (1969) measured a diffusion coefficient of $0{\cdot}6 \times 10^{-5}$ cm^2 s^{-1} for Na^+ in the cytoplasm of intact skeletal muscle fibres, about half the value in free solution, a difference they attributed to physical barriers rather than specific binding. These measurements all suggest that the majority of intra-axonal Na^+ is freely diffusible, but the apparent diffusion coefficient calculated in Fig. 5 may overestimate the true diffusion coefficient for Na^+ in intact axons, due to acceleration of Na^+ entry by injury currents and to reduction in viscosity caused by injury-associated disruption of axoplasmic structures.

Resealing of the axon membrane

Many studies have shown that resealing of mechanically lesioned membranes is facilitated by Ca^{2+} (Yawo & Kuno, 1985; Gallant, 1988; Xie & Barrett, 1991; Zev & Spira, 1993; Krause *et al.* 1994; Steinhardt *et al.* 1994; Howard, David & Barrett, 1995). Restoration of membrane integrity is thought to involve process retraction, constriction of the cut end, and either fusion of cut ends or formation of a tightly packed plug of membrane vesicles (Lucas, 1987; Fishman, Tewari & Stein, 1990; Spira *et al.* 1993; Krause *et al.* 1994). Resealing has some similarities to exocytosis (Steinhardt *et al.* 1994), and appears to be facilitated by

proteolytic breakdown of certain cytoskeletal elements (Xie & Barrett, 1991). We hypothesize that the development of a steep gradient of $[Na^+]_i$ within the injured axon in a region where $[Na^+]_i$ was previously uniformly high (Fig. 2) indicates a location of functional membrane resealing. As we had to view long lengths of axon, due to uncertainty about where this $[Na^+]_i$ gradient would develop, our images did not have sufficient resolution to clarify the morphology of this hypothesized resealing site. It is likely that this site involves a physical barrier rather than just a site of intense Na^+ pumping activity. If no physical barrier existed, then one would expect the dye fluorescent signals evoked by 340 nm excitation to continue to decrease on the proximal side of the gradient due to continued leakage of dye out of the cut end, whereas in fact there was a gradual increase in fluorescent signals proximal to the gradient. Thus the gradient of $[Na^+]_i$ developed together with a dye gradient.

In some injured axons the membrane seems to reseal at the cut end (e.g. squid and earthworm giant axons studied by Krause *et al.* 1994), whereas other injured axons appear to reseal at a distance from the cut end. Yawo & Kuno (1985) reported formation of a partition-like structure 50–300 μm from the cut end of cockroach giant axons, comparable to the 50–320 μm distance defined in our study by development of an intra-axonal $[Na^+]$ gradient. It is unclear whether the resealing site observed in our short-term study would correspond to the final resealing site of these axons *in situ*. Injured axons may reseal their membranes at multiple sites, and regions in which transmembrane ionic balance is restored in the short term may die at a later time. A hint of delayed die-back comes from comparison of dye-injection studies of transected Mauthner axons in larval lampreys, where Strautman *et al.* (1990) found that axonal filling stopped an average of 293 μm from the cut at 1 day post-transection, whereas Yin & Selzer (1983) found that axonal filling stopped 1–2 mm from the cut end at 12–20 days post-transection. Also, in our study the site and timing of resealing may have been influenced by the fact that these axons had been transected before at a distant site during the initial dissection of the preparation.

We had thought that resealing might occur preferentially at nodes of Ranvier, where the smaller axonal diameter might facilitate barrier formation, but the node was the resealing site in only one of the observed cases.

The timing of axonal resealing reported in the literature, as assayed by dye exclusion, decline of injury currents, or restoration of input resistance/membrane potential, varies from minutes to days. The range of 6–55 min reported here for lizard peripheral myelinated axons based on development of an intra-axonal $[Na^+]$ gradient is comparable to that of Howard *et al.* (1995) in their preliminary report that found that most lesioned rat peripheral myelinated axons reseal within 60 min based on dye exclusion. Van Egeraat & Wikswo (1993) calculated for a 25 mm long model of the transected squid giant axon that transmembrane ion gradients would dissipate if resealing times exceeded a critical resealing time constant of 135 s. The resealing times measured in our and other studies greatly exceeded this value, and as predicted, there was marked dissipation of the transmembrane $[Na^+]$ gradient and, by implication, the transmembrane $[K^+]$ gradient as well.

Recovery of $[Na^+]_i$

Amazingly, axonal regions whose $[Na^+]_i$ had exceeded 100 mM for 30 min or more were able to recover their normal resting $[Na^+]_i$ within about 1 h after resealing. As indicated in Fig. 6, part of this recovery was attributable to diffusional redistribution of Na^+ into regions more distant from the cut, but the rate of recovery, and the partial recovery of $[Na^+]_i$ observed in isolated segments, indicated an important contribution by active pumping as well. Thus regions lacking a transmembrane $[Na^+]$ gradient must retain sufficient ATP (or ATP-generating capacity) to permit active Na^+ extrusion. In injured axons pump activity might be expected to be reduced by loss of MgATP and elevation of $[Ca^{2+}]_i$ (McGeogh, 1990), but to be increased by membrane depolarization (Rakowski, Gadsby & De Weer, 1989), increased $[Na^+]_i$ and (probably) increased extra-axonal $[K^+]$.

It was interesting that active extrusion of Na^+ occurred even in axonal segments lacking a node. Cytochemical studies and most immunohistochemical studies using monoclonal antibodies and antisera against Na^+,K^+-ATPase have localized the majority of pump sites at nodes (reviewed by Sweadner, 1989), where action potential-associated Na^+ influx is localized, but at least one pump isoform is preferentially distributed in the internodal axolemma (Mata, Fink, Ernst & Siegel, 1991). Also, Bostock, Baker & Reid (1991) argued for internodal pump sites in their model for postischaemic changes in the excitability of human motor axons. Our results provide functional evidence that the internodal axolemma indeed has the ability to pump Na^+ and show that internodal $[Na^+]_i$ increases during intense stimulation.

Barrett, E. F. & Barrett, J. N. (1982). Intracellular recording from vertebrate myelinated axons: mechanism of the depolarizing afterpotential. *Journal of Physiology* **323**, 117–144.

Berdan, R. C., Easaw, J. C. & Wang, R. (1993). Alterations in membrane potential after axotomy at different distances from the soma of an identified neuron and the effect of depolarization on neurite outgrowth and calcium channel expression. *Journal of Neurophysiology* **69**, 151–164.

Borgens, R. B., Jaffe, L. F. & Cohen, M. J. (1980). Large and persistent electrical currents enter the transected lamprey spinal cord. *Proceedings of the National Academy of Sciences of the USA* **77**, 1209–1213.

Borzak, S., Reers, M., Arruda, J., Sharma, V. K., Sheu, S.-S., Smith, T. W. & Marsh, J. D. (1992). Na^+ efflux mechanisms in ventricular myoctyes: measurement of $[Na^+]_i$ with Na^+-binding benzofuran isophthalate. *American Journal of Physiology* **263**, H866–874.

Bostock, H., Baker, M. & Reid, G. (1991). Changes in excitability of human motor axons underlying post-ischaemic fasciculations: evidence for two stable states. *Journal of Physiology* **441**, 537–557.

Crank, J. (1975). *The Mathematics of Diffusion*. Oxford University Press, New York.

David, G., Barrett, J. N. & Barrett, E. F. (1995*a*). Post-transection changes in axoplasmic sodium ion concentration in vertebrate peripheral myelinated axons. *Society for Neuroscience Abstracts* **21**, 1003.

David, G., Modney, B., Scappaticci, K. A., Barrett, J. N. & Barrett, E. F. (1995*b*). Electrical and morphological factors influencing the depolarizing after-potential in rat and lizard myelinated axons. *Journal of Physiology* **489**, 141–157.

Donoso, P., Mill, J. G., O'Neill, S. C. & Eisner, D. A. (1992). Fluorescence measurements of cytoplasmic and mitochondrial sodium concentration in rat ventricular myocytes. *Journal of Physiology* **448**, 493–509.

Fishman, H. M., Tewari, K. P. & Stein, P. G. (1990). Injury-induced vesiculation and membrane redistribution in squid giant axon. *Biochimica et Biophysica Acta* **1023**, 421–435.

Gallant, P. E. (1988). Effects of the external ions and metabolic poisoning on the constriction of the squid giant axon after axotomy. *Journal of Neuroscience* **8**, 1479–1484.

Harootunian, A. T., Kao, J. P. Y., Eckert, B. K. & Tsien, R. Y. (1989). Fluorescence ratio imaging of cytosolic free Na^+ in individual fibroblasts and lymphocytes. *Journal of Biological Chemistry* **264**, 19458–19467.

Hinke, J. A. M. (1961). The measurement of sodium and potassium activities in the squid axon by means of cation-selective glass microelectrodes. *Journal of Physiology* **156**, 314–335.

Hodgkin, A. L. & Keynes, R. D. (1956). Experiments on the injection of substances into squid giant axons by means of a microsyringe. *Journal of Physiology* **131**, 592–616.

Howard, M. J., David, G. & Barrett, J. N. (1995). Calcium dependence of membrane resealing in transected myelinated rat axons. *Society for Neuroscience Abstracts* **21**, 1003.

Koh, D.-S., Jonas, P. & Vogel, W. (1994). Na^+-activated K^+ channels localized in the nodal region of myelinated axons of *Xenopus*. *Journal of Physiology* **479**, 183–197.

Krause, T. L., Fishman, H. M., Ballinger, M. L. & Bittner, G. D. (1994). Extent and mechanisms of sealing in transected giant axons of squid and earthworms. *Journal of Neuroscience* **14**, 6638–6651.

Kushmerick, M. J. & Podolsky, R. J. (1969). Ionic mobility in muscle cells. *Science* **166**, 1297–1298.

Lasser-Ross, N. & Ross, W. N. (1992). Imaging voltage and synaptically activated sodium transients in cerebellar Purkinje cells. *Proceedings of the Royal Society of London* B **247**, 35–39.

Lehning, E. J., Doshi, R., Isaksson, N., Stys, P. K. & LoPachin, R. M. Jr (1996). Mechanisms of injury-induced calcium entry into peripheral nerve myelinated axons: role of reverse sodium–calcium exchange. *Journal of Neurochemistry* **66**, 493–500.

LoPachin, R. M. Jr & Stys, P. K. (1995). Elemental composition and water content of rat optic nerve myelinated axons and glial cells: effects of *in vitro* anoxia and reoxygenation. *Journal of Neuroscience* **15**, 6735–6746.

Lucas, J. H. (1987). Proximal segment retraction increases the probability of nerve cell survival after dendrite transection. *Brain Research* **425**, 384–387.

Lucas, J. H., Gross, G. W., Emery, D. G. & Gardner, C. R. (1985). Neuronal survival or death after dendrite transection close to the perikaryon: correlation with electrophysiologic, morphologic, and ultrastructural changes. *Central Nervous System Trauma* **2**, 231–255.

Luther, P. W., Yip, R. K., Bloch, R. J., Ambesi, A., Lindenmayer, G. E. & Blaustein, M. P. (1992). Presynaptic localization of sodium/calcium exchangers in neuromuscular preparations. *Journal of Neuroscience* **12**, 4898–4904.

McGeoch, J. E. M. (1990). The α-2 isomer of the sodium pump is inhibited by calcium at physiological levels. *Biochemical and Biophysical Research Communications* **173**, 99–105.

McGill, D. L. (1991). Characterization of the adipocyte ghost (Na^+, K^+) pump: insights into the insulin regulation of the adipocyte (Na^+, K^+) pump. *Journal of Biological Chemistry* **266**, 15817–15823.

Marlier, L. N. J.-L., Zheng, T., Tang, J. & Grayson, D. R. (1993). Regional distribution in the rat central nervous system of a mRNA encoding a portion of the cardiac sodium/calcium exchanger isolated from cerebellar granule neurons. *Molecular Brain Research* **20**, 21–39.

Mata, M., Fink, D. J., Ernst, S. A. & Siegel, G. J. (1991). Immunocytochemical demonstration of Na^+,K^+-ATPase in internodal axolemma of myelinated fibers of rat sciatic and optic nerves. *Journal of Neurochemistry* **57**, 184–192.

Meiri, H., Spira, M. E. & Parnas, I. (1981). Membrane conductance and action potential of a regenerating axonal tip. *Science* **211**, 709–712.

Minta, A. & Tsien, R. Y. (1989). Fluorescent indicators for cytosolic sodium. *Journal of Biological Chemistry* **264**, 19449–19457.

Morita, K., David, G., Barrett, J. N. & Barrett, E. F. (1993). Posttetanic hyperpolarization produced by electrogenic Na^+–K^+ pump in lizard axons impaled near their motor terminals. *Journal of Neurophysiology* **70**, 1874–1884.

Nonner, D., Brass, B. J., Barrett, E. F. & Barrett, J. N. (1993). Reversibility of nerve growth factor's enhancement of choline acetyltransferase activity in cultured embryonic rat septum. *Experimental Neurology* **122**, 196–208.

Poulter, M. O., Hashiguchi, T. & Padjen, A. L. (1995). Evidence for a sodium-dependent potassium conductance in frog myelinated axon. *Neuroscience* **68**, 487–495.

Rakowski, R. F., Gadsby, D. C. & De Weer, P. (1989). Stoichiometry and voltage dependence of the sodium pump in voltage-clamped, internally dialyzed squid giant axon. *Journal of General Physiology* **93**, 903–941.

Rand, R. P., Fuller, N. L. & Lis, L. J. (1979). Myelin swelling and measurement of forces between myelin membranes. *Nature* **279**, 258–260.

Robinson, R. A. & Stokes, R. H. (1959). *Electrolyte Solutions*. Butterworths, London.

Rose, C. R. & Ransom, B. R. (1996). Intracellular sodium homeostasis in rat hippocampal astrocytes. *Journal of Physiology* **491**, 291–305.

Spira, M. E., Benbassat, D. & Dormann, A. (1993). Resealing of the proximal and distal cut ends of transected axons: electrophysiological and ultrastructural analysis. *Journal of Neurobiology* **24**, 300–316.

Steinhardt, R. A., Bi, G. & Alderton, J. M. (1994). Cell membrane resealing by a vesicular mechanism similar to neurotransmitter release. *Science* **263**, 390–393.

Strautman, A. F., Cork, R. J. & Robinson, K. R. (1990). The distribution of free calcium in transected spinal axons and its modulation by applied electrical fields. *Journal of Neuroscience* **10**, 3564–3575.

Sweadner, K. J. (1989). Isozymes of the Na^+/K^+-ATPase. *Biochimica et Biophysica Acta* **988**, 185–220.

VAN EGERAAT, J. M. & WIKSWO, J. P. JR (1993). A model for axonal propagation incorporating both radial and axial ionic transport. *Biophysical Journal* **64**, 1287–1298.

WANG, J. H. (1952). Tracer-diffusion in liquids. I. Diffusion of tracer amount of sodium ion in aqueous potassium chloride solution. *Journal of the American Chemical Society* **74**, 1182–1186.

XIE, X. Y. & BARRETT, J. N. (1991). Membrane resealing in cultured rat septal neurons after neurite transection: evidence for enhancement by Ca^{2+}-triggered protease activity and cytoskeletal disassembly. *Journal of Neuroscience* **11**, 3257–3267.

YAWO, H. & KUNO, M. (1985). Calcium dependence of membrane resealing at the cut end of the cockroach giant axon. *Journal of Neuroscience* **5**, 1626–1632.

YIN, H. S. & SELZER, M. E. (1983). Axonal regeneration in lamprey spinal cord. *Journal of Neuroscience* **3**, 1135–1144.

ZEV, N. E. & SPIRA, M. E. (1993). Spatiotemporal distribution of Ca^{2+} following axotomy and throughout the recovery process of cultured *Aplysia* neurons. *European Journal of Neuroscience* **5**, 657–668.

Acknowledgements

We thank Dr Wolfgang Nonner for reading a draft of this manuscript. This work was supported by grants from the NIH (NS 12404) and the American Paralysis Association, and by an equipment grant from the University of Miami.

Author's email address

G. David: gdavid@newssun.med.miami.edu

Received 19 August 1996; accepted 2 October 1996.